Carboxylated Cellulose Silica Hybrid Beads for Efficient Dye Removal

Qianqian Wang,[a,b,*] Simeng Liu,[b] Honglei Chen,[a] Jun Liu,[b] Huan Liu,[b] and Qianqian Zhu [b,c,*]

Highly efficient and environmentally friendly carboxylated cellulose silica hybrid adsorbents were prepared by combining the advantages of cellulose and silica. The surface property and chemical composition of produced cellulose silica hybrid adsorbents were extensively characterized *via* different techniques. The results indicated that silica particles were densely deposited on the surface of composite adsorbents. Because of their porous structure and large specific surface area, the carboxylated cellulose silica hybrid adsorbents demonstrated a high capacity of methylene blue (MB) adsorption, exceeding 990 mg·g^{-1}. This adsorption capacity was more than 45% higher than that of carboxylated cellulose adsorbent. The cellulose silica hybrid adsorbents were able to maintain an MB adsorption efficiency of up to 70% even after undergoing five cycles. This study developed cellulose silica hybrid adsorbents for wastewater treatments. High adsorption capacity and stability make them sustainable and cost-effective alternatives to traditional adsorbents.

INTRODUCTION

Cellulose adsorbents are attractive due to their high efficiency in removing various pollutants from wastewater (Varghese *et al.* 2019; Das *et al.* 2022). It is of great significance to develop cost-effective adsorbents from renewable and sustainable materials (Wang *et al.* 2022b). Nevertheless, natural cellulose possesses a dense structure containing a large number of crystalline regions, which do not offer a substantial number of active sites for adsorption (Rahman *et al.* 2018; Peter 2021; Wang *et al.* 2022c). Mechanical and chemical modifications of cellulose are commonly adopted to improve adsorption performance (Kaur *et al.* 2022). Microfibrillation and nanofibrillation can break down dense hydrogen bonds and van der Waals forces in pristine crystallized cellulose, thereby increasing its surface area and the number of hydroxyl groups on the surface (Liang *et al.* 2020). This enhances the adsorption capacity of cellulose-based materials by creating more active adsorption sites, making them highly effective adsorbents for heavy metals, dyes, and various other pollutants (Das *et al.* 2022). Chemical modifications are typically achieved through selective substitutions of the three free hydroxyl groups located on the C2, C3, and C6 positions of cellulose (Hokkanen *et al.* 2016). Commonly used methods for cellulose modification include oxidation, esterification, etherification, and copolymerization (Hokkanen *et al.* 2016). Those specifically designed cellulose

derivatives often exhibit excellent adsorption performances. The functional groups on cellulose derivatives can vary depending on the desired adsorption application. For example, 2,2,6,6-tetramethylpiperidine-1-oxyl (TEMPO) oxidation selectively introduces anionic carboxyl groups on the surfaces of cellulose at the C6 position, making cellulose an excellent adsorbent for various dyes and metals (Fiol *et al.* 2019). Amine groups can be added to increase the adsorption capacity for acidic gases (Hamdy *et al.* 2021).

To broaden the possible uses of cellulose-based adsorbents, cellulose-based inorganic hybrid composites are of great interest (Demilecamps *et al.* 2014; Rahmanian *et al.* 2021). Cellulose inorganic hybrids combine the properties of cellulose with those of inorganic materials, such as silica, alumina, and titanium oxide (Salama 2023). These hybrids can have enhanced mechanical, thermal, and adsorption properties compared to pure cellulose. For example, cellulose silica hybrids have been shown to have higher stability and increased adsorption capacity for heavy metals compared to pure cellulose (Agaba *et al.* 2018). The development of cellulose inorganic hybrid composites is a potential avenue to improve their properties and expand their potential applications.

In previous work, carboxylated cellulose beads were prepared with TEMPO-based oxidization and their kinetic adsorption behaviors were examined in detail (Wang *et al.* 2022a). The results indicated that carboxylated cellulose beads can effectively adsorb cationic dye because of the high surface area and strong electrostatic interactions. The present study attempts to further enhance the adsorption capacity of cellulose beads with silica incorporation. Thus, the fabricated cellulose silica hybrid beads were extensively characterized and the influences of silica on the properties of cellulose hybrid absorbents were examined. The adsorption performance and reusability of cellulose silica hybrid beads were examined with methylene blue (MB) as the model dye.

EXPERIMENTAL

Materials

Cotton linter obtained from Hubei Chemical Fiber Group Co., Ltd. (Xiangfan, China) with a viscosity-average molecular weight of 1.07×10^5 g/mol g·mol^{-1} was used as a raw material. Analytical grade 2,2,6,6-tetramethylpiperidine-1-oxyl radical (TEMPO), sodium bromide (NaBr), sodium hydroxide (NaOH), urea (CH_4N_2O), hydrochloric acid (HCl), ethanol (C_2H_6O), sodium hypochlorite (NaClO, 10% active chlorine), and sodium silicate nonahydrate ($Na_2SiO_3 \cdot 9H_2O$) were obtained from Sinopharm Chemical Reagent Co., Ltd. (Shanghai, China) and used as received.

Carboxylation and NaOH/urea Dissolution of Cellulose

The TEMPO-based oxidation and NaOH/urea dissolution of cellulose powder were conducted following the reported procedure (Wang *et al.* 2022a). Initially, 10 g cellulose powder was mixed in 1000 mL water with 1.0 g NaBr and 160 mg TEMPO. The oxidation immediately started with the dropwise addition of NaClO solution (70 mL). The pH was maintained at around 10. The reaction was quenched with ethanol addition. After filtering and washing, 3.5 g oxidized cellulose was dissolved in 100 g NaOH/urea solution (7 g NaOH and 12 g Urea in 81 g water) at -12 °C overnight. A transparent and viscous cellulose solution was obtained after vigorous stirring for 5 min.

bioresources.com

Fabrication of Carboxylated Cellulose Silica Hybrid Beads

Cellulose silica hybrid beads were fabricated by the falling-ball method (De Wever *et al.* 2022). First, sodium silicate nonahydrate solutions were prepared at different concentrations (8%, 10%, 12%, and 14%). Precooled (4 °C) sodium silicate solutions were then mixed with cellulose solution at a fixed ratio (1:1 w/w). Cellulose silica hybrid beads were prepared by the falling-ball method. Specifically, drops of the cellulose silica solution were injected into a 2 mol·L^{-1} HCl regeneration bath with a 5 mL syringe (the gauge of 2 mm) at a tip distance of 1 cm. Cellulose silica hybrid beads were thoroughly washed with pure water to constant pH (~7). The obtained cellulose silica hybrid beads were denoted as TCSB-8, TCSB-10, TCSB-12, and TCSB-14. The pristine cellulose beads were cellulose beads obtained via NaOH/urea dissolution without TEMPO surface modification. TEMPO-oxidized cellulose beads without silica addition were denoted as TCSB-0.

Characterization of Cellulose Silica Hybrid Beads

For instrument characterizations, cellulose silica hybrid beads were freeze-dried (Martin Christ Beta1-8 LD plus, Osterode am Harz, Germany). The dry content of cellulose silica beads was determined before freeze-drying and after. The cellulose silica hybrid beads were characterized by scanning electron microscopy (SEM), thermogravimetric analysis (TGA), Fourier transform infrared (FTIR) spectroscopy, X-ray diffraction (XRD), Brunauer-Emmet-Teller (BET) method, and X-ray photoelectron spectroscopy (XPS). A JSM-7800F SEM (JEOL, Tokyo, Japan) equipped with an energy-dispersive X-ray (EDAX LLC, Mahwah, NJ, USA) was used to characterize bead morphologies and silica contents. The sample was attached to an aluminum stub using carbon tape and gold-coated. The surface of the cellulose silica bead was imaged at 20 kV. The TGA was conducted to determine the thermal stability of cellulose silica hybrid beads using a Perkin Elmer TGA 4000 instrument (Waltham, MA, USA) under a nitrogen atmosphere over the temperature range of 30 °C to 800 °C with a heating rate of 20 °C·min^{-1}. The FTIR spectroscopic studies were performed with a Thermo Nicolet Nexus 470 FTIR spectrometer (Waltham, MA, USA) scanned in the range of 4000 to 500 cm^{-1} with a resolution of 4 cm^{-1}. The X-ray diffraction (XRD) studies were conducted with a Bruker D8 Advance diffractometer (Billerica, MA, USA), equipped with Cu Kα radiation ($\lambda = 0.1541$ nm) as the X-ray source. The surface area was determined by the BET method with a Micromeritics TriStar II automated system (Norcross, GA, USA). Elemental composition and chemical bonding states of cellulose silica hybrid beads were examined in an AXIS-Ultra DLD (Kratos, Shimadzu, Japan) XPS.

Methylene Blue Adsorption Evaluation

The adsorption performances of cellulose silica hydrogel beads were evaluated with MB dye (Wang *et al.* 2022a). For each experiment, a certain amount (20 mg) of cellulose beads were added to a conical flask filled with 100 mL MB (200 mg·L^{-1}, unless otherwise stated) solution and then shaken at 160 rpm from 25 °C until equilibrium. The MB concentration was quantitatively determined at 662 nm with a UV-2600 spectrophotometer (Shimadzu, Japan). The amount of MB adsorbed was calculated from the difference between the initial and equilibrium concentrations.

Equilibrium adsorption capacity $\qquad q_e = \frac{(c_0 - c_e)}{m} \cdot V \qquad\qquad$ (1)

where c_0 and c_e are the initial and equilibrium concentrations (mg·L^{-1}) of MB; q_e is the adsorption capacities (mg·g^{-1}) at equilibrium.

RESULTS AND DISCUSSION

Properties of Carboxylated Cellulose Silica Hybrid Beads

It is known that cellulose fibers can act as templates for silica particles (Wang *et al.* 2022d). In this study, the viscous cellulose silica solution spontaneously solidified into a microsphere within seconds after dropping into the regeneration bath. Simultaneously, silica particles form and accumulate on the surface of coagulated cellulose or inside the pores through a neutralization and condensation process (Demilecamps *et al.* 2014). Cellulose silica hybrid beads with diameters around 3.5 mm were fabricated.
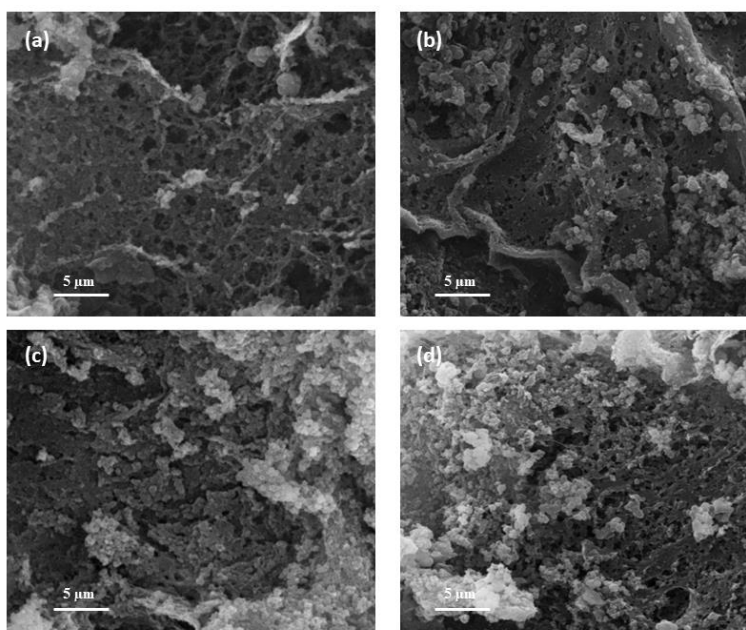
Fig. 1. SEM images of cellulose silica hybrid beads with different silica loadings: (a) TCSB-8; (b) TCSB-10; (c) TCSB-12; and (d) TCSB-14

The SEM images of cellulose silica hybrid beads provide important insights into their morphology and structure. Freeze-dried cellulose silica hybrid beads were spray coated with gold and the surfaces of the beads were imaged, as shown in Fig. 1. The cellulose solution is viscous and when it comes into contact with the antisolvent, regenerated cellulose beads with inner fibrous structures were immediately formed (Wang *et al.* 2022a). The introduction of silica had obvious influences on the morphology of cellulose silica hybrid beads. When the silica precursor was added at a low loading of 8%, small silica particles were homogeneously dispersed in the cellulose matrix. Increasing the silica precursor to 10% resulted in larger silica particles in the hybrid beads, which were more visible compared to the previous loading (Fig. 1a *vs*. Fig. 1b). Further increasing the silica precursor loading to 14% resulted in the formation of large silica aggregates (Fig. 1d).

Table 1. SEM-EDS Data for Selected Points of Cellulose Silica Hybrid Beads with Different Silica Loadings

Sample ID	C (%)	O (%)	Si (%, EDS)	Si (%, TGA)
TCSB-0	50.11	49.89	-	-
TCSB-8	52.17	45.78	2.05	21.97
TCSB-10	52.80	42.77	4.16	26.13
TCSB-12	26.23	55.99	17.78	29.71
TCSB-14	21.66	54.35	22.72	33.12

The energy-dispersive X-ray spectroscopy indicated that the sample mainly consisted of C, O, and Si. The silica contents in the hybrid beads were estimated at the selected points (Table 1). However, the determined silica contents were not consistent with that estimated by TGA (Fig. 2a and 2b). The intensities of the X-ray elemental peaks were site-sensitive. Thus, the site-specific point scan is unable to identify the average silica content effectively due to the uneven distribution of silica in the hybrid beads. Further study will conduct an area scan, which may be more representative and comparable.
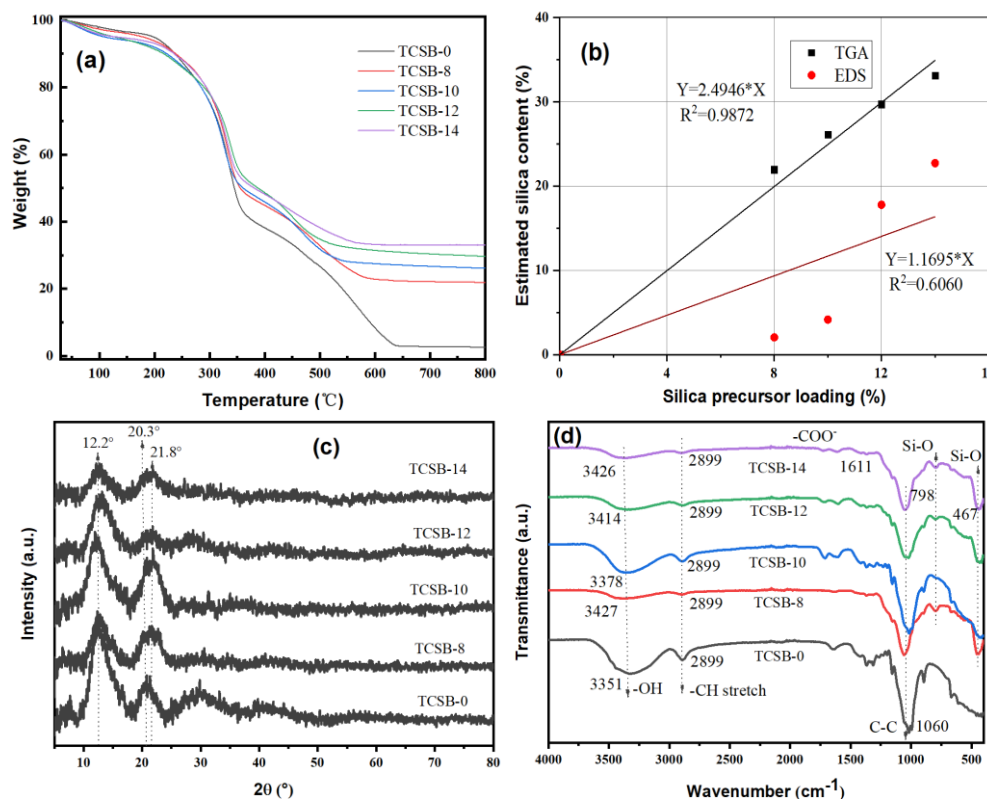
Fig. 2. (a) TGA curves, (b) estimated silica content, (c) XRD, and (d) FTIR spectra of cellulose silica hybrid beads with different silica loadings

TGA profiles of cellulose silica hybrid beads with various silica loadings are displayed in Fig. 2a. The weight loss below 120 °C predominantly results from the loss of water in the beads, implying that the freeze-dried cellulose silica hybrid beads exhibit relatively high hydrophilicity and hygroscopicity (Quan *et al.* 2021). The predominant weight loss primarily arises from the decomposition of cellulose (Jia *et al.* 2011). The introduction of silica does not affect the thermal decomposition temperature of the

cellulose. The weight remains essentially unchanged after cellulose decomposition because silica is stable at higher temperatures, the silica content in cellulose silica hybrid beads can be roughly estimated from the residual weight (Feng *et al.* 2016). Based on the TGA curves depicted in the Fig. 2b, the silica contents in TCSB-8, TCSB-10, TCSB-12, and TCSB-14 were 22.0%, 26.1%, 29.7%, and 33.1%, respectively. It can be found that the silica contents linearly rose with the increasing loading of sodium silicate in cellulose solution (R^2 = 0.9872). These outcomes validate the successful incorporation of silica in cellulose hybrid beads.

X-ray diffraction patterns of cellulose silica hybrid beads are shown in Fig. 2c. It can be observed that the main diffraction peak positions for cellulose silica hybrid beads were roughly the same as those for pure cellulose beads. Specifically, cellulose II characteristic peaks corresponding to (1-10), (110), and (020) crystal planes were observed at 2θ = 12.2°, 20.3°, and 21.8°, respectively (Wang *et al.* 2022a). It is worth mentioning that no silica diffraction peaks were detected in the X-ray diffraction patterns. This suggests that the silica present in the beads is amorphous, meaning that it lacks long-range order and does not have a well-defined crystal structure (Feng *et al.* 2016).

FTIR spectra of cellulose silica hybrid beads are illustrated in Fig. 2d. The peak at 3351 cm^{-1} is attributed to the characteristic hydrogen bondings present in cellulose (Jiang and Hsieh 2016). The symmetric stretching vibration of C-H was observed at roughly 2899 cm^{-1}, and that of the carboxyl group was found at 1611 cm^{-1} (Jiang and Hsieh 2016). In comparison with the FTIR spectrum of pure cellulose, novel characteristic peaks were observed for cellulose silica hybrid beads. The Si-O bending and contraction peaks were detected at 798 and 467 cm^{-1}, implying that silica was successfully deposited on cellulose hybrid beads (Rahmatika *et al.* 2019). The intensity of the Si-O peak increases and the position shifts slightly with the gradual rise in the mass fraction of silica.

Variations in the BET surface area and pore sizes of cellulose silica hybrid beads are shown in Table 2. The formation and precipitation of silica particles on the surface of cellulose affect the surface area and internal pore structure of cellulose hybrid beads. As the mass fraction of silicate precursor in the solution increased, the loading of silica particles on the surface of cellulose gradually increased, leading to a gradual increase in BET surface area and a decrease in the average pore diameter. The maximum BET surface area reached 229.4 m$^2 \cdot$g^{-1}, and the pore diameter decreased to 3.61 nm for TCSB-14. Large specific surface area, high porosity, and small pore diameter make cellulose silica hybrid beads highly favorable for adsorption applications.

Table 2. Surface Area and Pore Sizes of Cellulose Silica Hybrid Beads

Sample ID	Average Diameter of Hydrogel Beads (mm)	BET Surface Area (m$^2 \cdot$g^{-1})	BET Mean Pore Size (nm)
TCSB-0	3.51	105.78	4.02
TCSB-8	3.35	127.63	4.02
TCSB-10	3.29	185.51	4.01
TCSB-12	3.40	188.48	3.96
TCSB-14	3.35	229.44	3.61

Evaluation of MB Adsorption onto Carboxylated Cellulose Silica Hybrid Beads

Methylene blue was used as a model dye to evaluate the adsorption performances of cellulose silica hybrid beads. The success of MB removal from aqueous solutions by adsorption depends on various factors including adsorbent property, pH of the solution, equilibrium time, and temperature (Hokkanen *et al.* 2016).
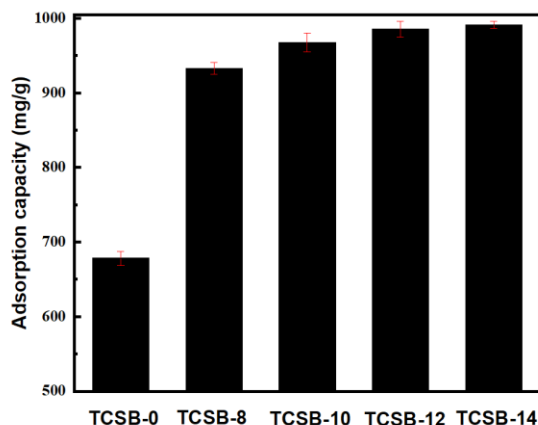
Fig. 3. Effect of SiO_2 content on MB removal rate

Initially, the impact of silica loading on the performance of cellulose silica hybrid beads was assessed. The adsorption capacity of cellulose beads was then evaluated. As depicted in Fig. 3, the introduction of silica led to an increase in the adsorption capacity for MB. The adsorption capacity of the pure cellulose adsorbent (TCSB-0) was 678 $mg \cdot g^{-1}$. The adsorption capacity of pure cellulose in the same range (579 to 917 $mg \cdot g^{-1}$) was also reported (Zhang *et al.* 2022). With an increase in silica loading, the adsorption capacity gradually rose, reaching a maximum of 995 $mg \cdot g^{-1}$ for TCSB-14. The elevated adsorption capacity was attributed to the synergistic effect of carboxylated cellulose and silica particles with substantial surface areas.

The influences of other factors, such as adsorbent loading, adsorption time, pH, and temperature, on the performance of carboxylated cellulose silica hybrid beads were examined. Cellulose silica hybrid beads loading was investigated in the range of 10 mg to 30 mg (Fig. 4a). An adsorbent weight of 20 mg exhibited a high removal performance. The adsorption capacity decreased as the amount of adsorbent increased because more active adsorptive sites remained unsaturated. It was noted that cellulose silica hybrid beads take a long time to reach adsorption equilibrium. Within the first hour, the absorption rate is relatively fast. As the adsorption proceeds, the absorption rate starts to slow down and reaches equilibrium after 4 h (Fig. 4b).

The MB removal was also influenced by the pH of the solution (Fig. 4c). With the increase of pH from 3 to 8, there was a clear increasing trend of the MB removal effectiveness. However, when the pH continues to rise to 12, the MB removal rate began to slowly decrease. Despite this decrease, the removal was still higher compared to acidic conditions. This is because the pH can affect the surface charge of the adsorbent and the charge of the adsorbate, which can impact the strength of the electrostatic forces that drive the adsorption process. A slight decrease in the adsorption capacity was detected with

increasing temperature (Fig. 4d). This phenomenon can be attributed to the desorption of the adsorbed molecules from the surface of the beads at elevated temperatures.
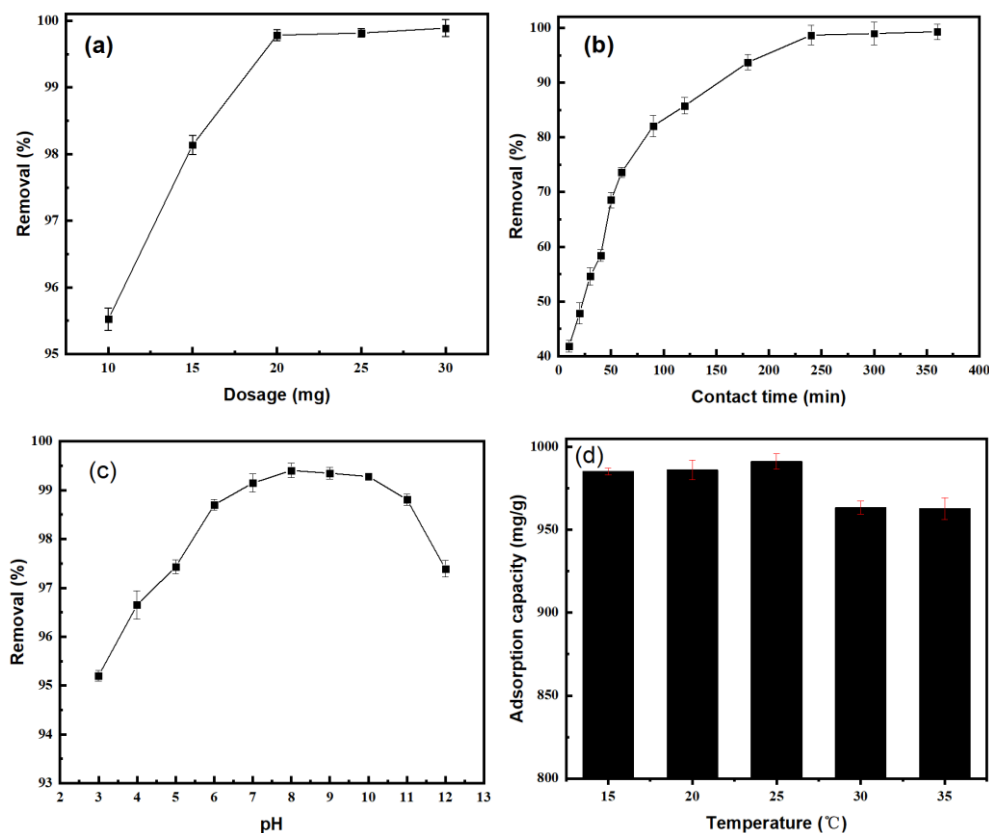
Fig. 4. Effects of (a) adsorbent loading, (b) time, (c) pH, and (d) temperature on adsorption performance of cellulose silica hybrid beads (TCSB-14). All the experimental parameters are the same besides the one examined. Bead loading: 20 mg; pH: 7; temperature: 25 °C; time: 4 hours.

This study also examined the potential for reusing carboxylated cellulose silica hybrid beads by subjecting them to a straightforward washing process using 10 mL 1.0 mol·L^{-1} NaOH solution as the eluent. The adsorption-desorption process was repeated five times, and the adsorption capacity was measured for each cycle. The recycling performances, depicted in Fig. 5, demonstrate that the cellulose silica hybrid beads maintained an adsorption capacity of over 70% after five cycles of the adsorption-desorption process. These findings suggest good recycling capabilities for the hybrid beads. The loss of adsorption capacity from 997 to 726 mg·g^{-1} may be due to the physical degradation of cellulose silica hybrid beads caused by repeated use. Fewer active sites are available after multiple adsorption-desorption processes.

The surface chemical composition of pristine cellulose beads (CB), TEMPO-oxidized cellulose beads (TCB), and cellulose silica hybrid beads (TCSB-14) before and after MB adsorption were determined using XPS analysis. As displayed in Fig. 6, the spectrum of pristine cellulose beads revealed only characteristic peaks of C 1s at 285.9 eV and O 1s at 532.6 eV, which were consistent with other reports (Johansson *et al.* 2020). A new characteristic peak corresponding to the Na 1s energy spectrum appeared at 1071.9 eV after TEMPO oxidation. For the silica-functionalized cellulose hybrid beads, new peaks with binding energies of 154.5 eV (Si 2s) and 103.1 eV (Si 2p) appeared, indicating the

successful deposition of silica in cellulose hybrid beads. After MB was adsorbed onto the cellulose silica hybrid bead, the Na 1s energy spectrum peak disappeared, and the intensities of Si 2s and Si 2p energy spectrum peaks decreased. The C1s peak of pristine cellulose beads can be deconvoluted into three peaks located at 288.0 eV for O-C-O, 286.4 eV for C-O, and 284.7 eV for C-C (Awada *et al.* 2012). After TEMPO oxidation, a new C1s deconvoluted peak at 288.3 eV for O-C=O appeared (Awada *et al.* 2012). After the adsorption of MB onto cellulose silica hybrid beads, a new energy spectrum peak for C-N appears, indicating the successful adsorption of MB by the cellulose silica hybrid beads.
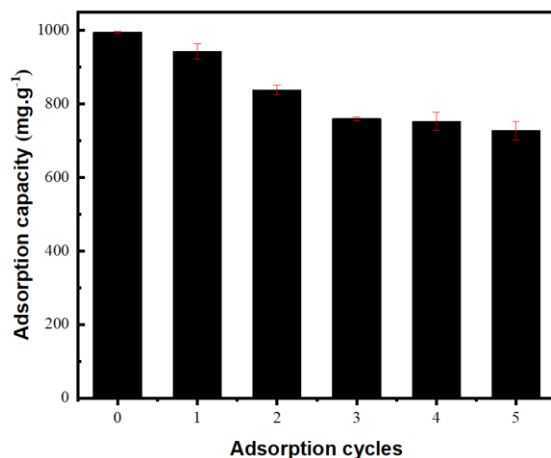
Fig. 5. Effect of adsorption cycles on the performance adsorption of MB by TCSB-14
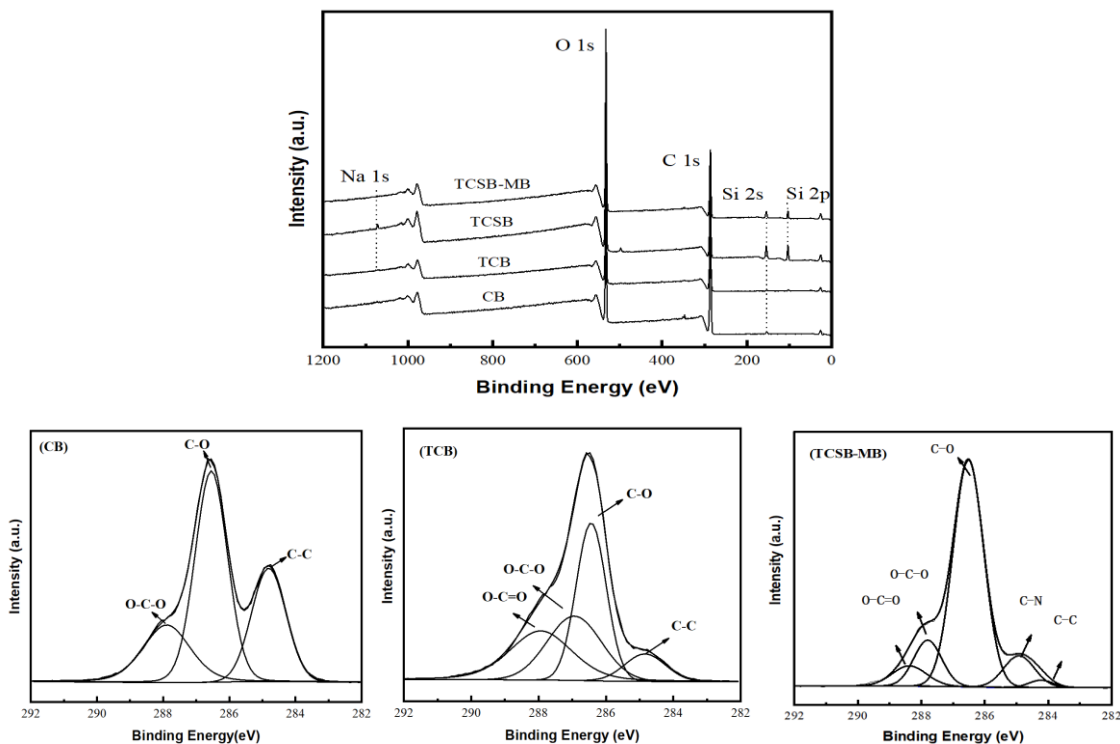
Fig. 6. XPS wide scan of cellulose beads with XPS energy spectrum of C 1s

CONCLUSIONS

1. Carboxylated cellulose silica hybrid beads were fabricated by the falling-ball technique. Different amounts of silica were introduced into cellulose hybrid beads. The amount of silica introduced into cellulose hybrid beads influence their structures and properties.

2. The increase in the silica content of carboxylated cellulose silica hybrid beads resulted in an increase in their specific surface area and a decrease in pore size. The carboxylated cellulose beads, in the absence of silica, had a specific surface area of 106 $m^2 \cdot g^{-1}$ and an average pore size of 4.02 nm. Upon the introduction of silica, the maximum specific surface area increased to 229 $m^2 \cdot g^{-1}$, concomitant with a reduction in the average pore size to 3.61 nm.

3. The high surface area made them effective for adsorbing dye molecules from aqueous solutions. The adsorption capacity of carboxylated cellulose silica hybrid beads (TCSB-14) exceeded 990 $mg \cdot g^{-1}$. The adsorption capacity of MB was still above 700 $mg \cdot g^{-1}$ after 5 cycles. The XPS characterization indicated the interactions between the hybrid bead and MB molecules.

4. Carboxylated cellulose silica hybrid beads have shown promising adsorption capacity, indicating their potential for use in wastewater treatment. Further research is necessary to optimize their properties for practical applications.

ACKNOWLEDGMENTS

REFERENCES CITED

Agaba, A., Cheng, H., Zhao, J., Zhang, C., Tebyetekerwa, M., Rong, L., Sui, X., and Wang, B. (2018). "Precipitated silica agglomerates reinforced with cellulose nanofibrils as adsorbents for heavy metals," *RSC Advances* 8(58), 33129-33137. DOI: 10.1039/C8RA05611K

Awada, H., Monplaisir, D., and Daneault, C. (2012). "Growth of polyelectrolyte on lignocellulosic fibres: Study by ζ-potential, ftir, and xps," *BioResources* 7(2), 2090-2104. DOI: 10.15376/biores.7.2.2090-2104

Das, R., Lindstrom, T., Sharma, P. R., Chi, K., and Hsiao, B. S. (2022). "Nanocellulose for sustainable water purification," *Chemical Reviews* 122(9), 8936-9031. DOI: 10.1021/acs.chemrev.1c00683

De Wever, P., Janssens, J., and Fardim, P. (2022). "Fabrication of cellulose cryogel beads via room temperature dissolution in onium hydroxides," *Carbohydrate Polymer Technologies and Applications* 3, article ID 100206. DOI: 10.1016/j.carpta.2022.100206

***bioresources*.com**

Demilecamps, A., Reichenauer, G., Rigacci, A., and Budtova, T. (2014). "Cellulose–silica composite aerogels from "one-pot" synthesis," *Cellulose* 21(4), 2625-2636. DOI: 10.1007/s10570-014-0314-3

Feng, J., Le, D., Nguyen, S. T., Tan Chin Nien, V., Jewell, D., and Duong, H. M. (2016). "Silica cellulose hybrid aerogels for thermal and acoustic insulation applications," *Colloids and Surfaces A: Physicochemical and Engineering Aspects* 506, 298-305. DOI: 10.1016/j.colsurfa.2016.06.052

Fiol, N., Vásquez, M. G., Pereira, M., Tarrés, Q., Mutjé, P., and Delgado-Aguilar, M. (2019). "TEMPO-oxidized cellulose nanofibers as potential cu(ii) adsorbent for wastewater treatment," *Cellulose* 26(2), 903-916. DOI: 10.1007/s10570-018-2106-7

Hamdy, L. B., Goel, C., Rudd, J. A., Barron, A. R., and Andreoli, E. (2021). "The application of amine-based materials for carbon capture and utilisation: An overarching view," *Materials Advances* 2(18), 5843-5880. DOI: 10.1039/d1ma00360g

Hokkanen, S., Bhatnagar, A., and Sillanpaa, M. (2016). "A review on modification methods to cellulose-based adsorbents to improve adsorption capacity," *Water Research* 91, 156-173. DOI: 10.1016/j.watres.2016.01.008

Jia, N., Li, S.-M., Ma, M.-G., Zhu, J.-F., and Sun, R-C. (2011). "Synthesis and characterization of cellulose-silica composite fiber in ethanol/water mixed solvents," *BioResources* 6(2), 1186-1195. DOI: 10.15376/biores.6.2.1186-1195

Jiang, F., and Hsieh, Y.-L. (2016). "Self-assembling of TEMPO oxidized cellulose nanofibrils as affected by protonation of surface carboxyls and drying methods," *ACS Sustainable Chemistry and Engineering* 4(3), 1041-1049. DOI: 10.1021/acssuschemeng.5b01123

Johansson, L.-S., Campbell, J. M., and Rojas, O. J. (2020). "Cellulose as the *in situ* reference for organic xps. Why? Because it works," *Surface and Interface Analysis* 52(12), 1134-1138. DOI: 10.1002/sia.6759

Kaur, J., Sengupta, P., and Mukhopadhyay, S. (2022). "Critical review of bioadsorption on modified cellulose and removal of divalent heavy metals (Cd, Pb, and Cu)," *Industrial and Engineering Chemistry Research* 61(5), 1921-1954. DOI: 10.1021/acs.iecr.1c04583

Liang, L., Bhagia, S., Li, M., Huang, C., and Ragauskas, A. J. (2020). "Cross-linked nanocellulosic materials and their applications," *ChemSusChem* 13(1), 78-87. DOI: 10.1002/cssc.201901676

Peter, Z. (2021). "Order in cellulosics: Historical review of crystal structure research on cellulose," *Carbohydrate Polymers* 254, article ID 117417. DOI: 10.1016/j.carbpol.2020.117417

Quan, H., Kisailus, D., and Meyers, M. A. (2021). "Hydration-induced reversible deformation of biological materials," *Nature Reviews Materials* 6(3), 264-283. DOI: 10.1038/s41578-020-00251-2

Rahman, N. S. A., Yhaya, M. F., Azahari, B., and Ismail, W. R. (2018). "Utilisation of natural cellulose fibres in wastewater treatment," *Cellulose* 25(9), 4887-4903. DOI: 10.1007/s10570-018-1935-8

Rahmanian, V., Pirzada, T., Wang, S., and Khan, S. A. (2021). "Cellulose-based hybrid aerogels: Strategies toward design and functionality," *Advanced Materials* 33(51), article ID 2102892. DOI: 10.1002/adma.202102892

Rahmatika, A. M., Goi, Y., Kitamura, T., Widiyastuti, W., and Ogi, T. (2019). "TEMPO-oxidized cellulose nanofiber (tocn) decorated macroporous silica particles: Synthesis,

characterization, and their application in protein adsorption," *Materials Science and Engineering: C* 105, article ID 110033. DOI: 10.1016/j.msec.2019.110033

Salama, A. (2023). "Novel cellulose/silica microspheres as sustainable and efficient adsorbents for methyl orange removal," *Fibers and Polymers* (Online). DOI: 10.1007/s12221-023-00139-2

Varghese, A. G., Paul, S. A., and Latha, M. S. (2019). "Remediation of heavy metals and dyes from wastewater using cellulose-based adsorbents," *Environmental Chemistry Letters* 17(2), 867-877. DOI: 10.1007/s10311-018-00843-z

Wang, Q., Liu, S., Chen, H., Liu, J., and Zhu, Q. (2022a). "TEMPO-oxidized cellulose beads for cationic dye adsorption," *BioResources* 17(4), 6056-6066. DOI: 10.15376/biores.17.4.6056-6066

Wang, Q., Liu, S., Liu, J., Sun, J., Zhang, Z., and Zhu, Q. (2022b). "Sustainable cellulose nanomaterials for environmental remediation - Achieving clean air, water, and energy: A review," *Carbohydrate Polymers* 285, article ID 119251. DOI: 10.1016/j.carbpol.2022.119251

Wang, Q., Zhou, R., Sun, J., Liu, J., and Zhu, Q. (2022c). "Naturally derived Janus cellulose nanomaterials: Anisotropic cellulose nanomaterial building blocks and their assembly into asymmetric structures," *ACS Nano* 16(9), 13468-13491. DOI: 10.1021/acsnano.2c04883

Wang, Q., Zhou, R., Liu, S., Sethupathy, S., Liu, J., Sun, J., Zou, L., and Zhu, Q. (2022d). "Templated synthesis and assembly with sustainable cellulose nanomaterial for functional nanostructure," *Cellulose* 29(8), 4287-4321. DOI: 10.1007/s10570-022-04577-8

Zhang, T., Xiao, S., Fan, K., He, H., and Qin, Z. (2022). "Preparation and adsorption properties of green cellulose-based composite aerogel with selective adsorption of methylene blue," *Polymer* 258, article 125320. DOI: 10.1016/j.polymer.2022.125320